ADVANCED MATERIALS

Supporting Information

for *Adv. Mater.*, DOI 10.1002/adma.202313663

Stereo-Hindrance Engineering of A Cation toward <110>-Oriented 2D Perovskite with Minimized Tilting and High-Performance X-Ray Detection

Mengling Xia, Xijuan Sun, Fan Ye, Mingquan Liao, Jiaqi Liu, Shiyou Liu, Dong Wu, Yinsheng Xu, Xianghua Zhang, Kan-Hao Xue*, Xiangshui Miao, Jiang Tang and Guangda Niu**

Stereo-hindrance Engineering of A Cation toward <110>-oriented 2D Perovskite with Minimized Tilting and High-performance X-ray Detection

Mengling Xia[*]*, Xijuan Sun, Fan Ye, Mingquan Liao, Jiaqi Liu, Shiyou Liu, Dong Wu, Yinsheng Xu, Xianghua Zhang, Kan-Hao Xue*[*]*, Xiangshui Miao, Jiang Tang, Guangda Niu*[*]

Prof. M. Xia, X. Sun, M. Liao, J. Liu, Dr. D. Wu, Prof. Y. Xu, Prof. X. Zhang
School of Materials Science and Engineering & State Key Laboratory of Silicate Materials for Architectures, Wuhan University of Technology, Wuhan 430070, China
E-mail: xiamengling@whut.edu.cn (M. Xia)

F. Ye, S. Liu, Prof. K. Xue, Prof. J. Tang, Prof. G. Niu
Wuhan National Laboratory for Optoelectronics (WNLO), Huazhong University of Science and Technology (HUST), Wuhan 430074, China
E-mail: guangda_niu@hust.edu.cn (G. Niu)

Prof. K. Xue, Prof. X. Miao
School of Integrated Circuits, Huazhong University of Science and Technology (HUST), Wuhan 430074, China
E-mail: xkh@hust.edu.cn (K. Xue)

Prof. X. Zhang
Laboratoire des Verres et Céramiques, UMR-CNRS 6226, Sciences chimiques de Rennes, Université de Rennes 1, Rennes 35042, France

Experimental section

Materials: Lead bromide (99.999%) was purchased from Advanced Election technology Co. Ltd. Hydrobromic acid (HBr) (40%) was purchased from Aladdin Chemical Co. Ltd. 1-ethylpiperazine was purchased from Shanghai Titan Scientific Co. Ltd. 1,4-diaminobutane (98%) was purchased from Shanghai Mackling Biochemical Co. Ltd. N, N-dimethylformamide (DMF) was purchased from Sinopharm Chemical Reagent Co., Ltd. All the chemicals were used as received without any further purification.

Single crystal synthesis: $EPZPbBr_4$ single crystal was synthesized by solution temperature-lowering (STL) method. Firstly, 3 mmol (1.1 g) $PbBr_2$ and 3 mmol (0.383 ml) 1-ethylpiperazine was dissolved in 4 ml and 1 ml HBr, respectively, to obtain solution A and B. Secondly, A and B solution was oscillatory mixed evenly to prepare precursor solution. Then, the precursor solution in reagent bottle was sealed by PVC tape and heated by 100 ℃ until totally dissolved. The transparent yellow solution was cooled at a rate of 1 ℃/h to facilitate the crystals growth.

$BDAPbBr_4$ single crystal was synthesized by solvent evaporation method. Firstly, 5 mmol $PbBr_2$ was dissolved in 30 ml DMF and then 2 ml 1,4-diaminobutane was added into the solution. After the white sediment formed, HBr was added drop by drop into the turbid solution under intense stirring until the pH of the solution reaching mildly acidic. The solution gradually turned clear at the mildly acidic condition. After stirring for half an hour, the solution was filtered into a clean beaker. The beaker was then covered by a piece of aluminum foil with several small holes. Finally, the beaker was heated at 60 ℃ for solvent evaporation through the small holes. Afterwards, the crystals continued to grow and they were harvested after one or two days.

Materials characterizations: Single crystal XRD measurements were performed using an X-ray diffractometer (XtaLAB PRO MM007HF) equipped with cryogenic liquid nitrogen system and with Cu K_α as the source. Powder XRD measurement was performed by a Rigaku MiniFlex600 X-ray diffractometer equipped with a Cu K_α X-ray (λ = 1.54186 Å) tube operated at 40 kV and 15 mA at a scanning step of ≈0.08° s^{-1}.The absorption spectra were recorded using UV-Vis-NIR spectrophotometer

(Lambda 750 S) in transmission mode. Time-resolved PL spectra were tested by a time-resolved fluorescence spectrometer (Spirit 1040-8-SHG06900 fR Rack LCR1) monitored at 560 nm under a 400 nm-pulse-laser as the excitation source. The temperature dependent PL spectra were conducted using Steady-state/Lifetime spectrofluorometer (QuantaMaster 8000) excited by Xenon lamp at 389 nm wavelength at a temperature ranging from 115K to 295K using a liquid-nitrogen cooler. The X-ray photoelectron spectra (XPS) were recorded using spectroscopy (ESCALAB 250Xi) with a monochrome Al target. The ultraviolet photoelectron spectra (UPS) were recorded by a spectroscopy (ESCALAB 250Xi). The excitation source was a HeI (21.22 eV) discharge lamp. The nanoindentation measurements were performed by Bruker-Hysitron TI-980 using a Berkovich indenter (three-sided pyramid-shaped tip). Four points were tested for each crystal.

Device Fabrication: Before device fabrication, the contaminations and the imperfect surface was removed through repeatedly lifting the crystal by ordinary tapes. To make planar structured photodetectors, bar-shaped Au electrodes with the thickness of 80 nm were deposited onto the one surface of the single crystals by thermally evaporating with the pre-designed shadow mask. The channel length between two Au electrodes was 1 mm. To make out-of-plane structured photodetectors, square Au electrodes were deposited onto the upper and bottom surface of the single crystals symmetrically. The distance between the electrodes is the thickness of the single crystals. The effective electrode area of $EPZPbBr_4$, $BDAPbBr_4$ and $EDBEPbBr_4$ X-ray detector was 0.0198 cm^2, 0.019 cm^2, and 0.032 cm^2, respectively.

X-ray detector performance measurement: The X-ray detection performance was measured on a homemade measurement system housed in the dark chamber to eliminate the impact of ambient light sources. A metal-ceramic X-ray tube (Moxtek MAGPRO 70 kV 12 W) was used as the X-ray source. X-ray photons were generated under the acceleration voltage of 50 kV with the operational current tuned from 20 to 140 μA. The distance between the X-ray tube and the detector was tuned from 10 to 80 cm. 1 mm-thick Al plates were used as attenuators to adjust the radiation dose rate. An electrometer (Keithley 6571B) was used to apply bias voltage on $EPZPbBr_4$ device and

collect the response current. The X-ray dose rate was calibrated with an ion chamber dosimeter (MagicMax from IBA DOSIMETRY).

Computational calculations: The density functional theory calculations were carried out using the Vienna Ab initio Simulation Package[1, 2] (VASP 5.4.4). The generalized gradient approximation (GGA) within the Perdew-Burke-Ernzerhof (PBE) functional form was used for the exchange-correlation energy, and projector augmented-wave (PAW) pseudopotentials were used to replace the core electrons. The plane wave energy cutoff was fixed to be 500 eV. The energy convergence criterion is 10^{-5} eV and the convergence criterion of force is 0.02 eV $Å^{-1}$. Geometry optimization was carried out using the Brillouin zone sampling scheme based on a 5×4×3 Monkhorst-Pack k-mesh Brillouin zone sampling scheme.

For better lattice parameter prediction, we adopted the PBEsol functional of the generalized gradient approximation (GGA) form to account for the exchange-correlation. The projector augmented-wave method[3, 4] was used, while the electrons considered as in the valence were: 1s for H; 2s and 2p for C, N; 4s and 4p for Br; 6s and 6p for Pb. The plane wave kinetic energy cutoff was fixed to 500 eV. A 3×3×2 -centered Monkhorst–Pack k-point grid[5] was used for Brillouin zone sampling in supercells. For electronic structure calculations, the self-energy corrected shell DFT-1/2 method[6, 7] was used, with −1/2 e correction done for Br anions only. The power index p in the cutoff function of DFT-1/2 equals 20[8].

For $EPZPbBr_4$ calculations, the lattice parameters were fixed to experimental values, with atomic coordinates fully optimized. The resulting stress level along each direction is less than 1.2 GPa, confirming the good performance of the PBEsol functional in terms of lattice parameters. When the EPZ^{2+} cations were replaced by smaller or bigger organic cations, the lattice parameters were also optimized to minimize the residue stress.

Statistical Analysis: All experimental data were converted and plotted through the Origin 8.5 program. The crystal structures were processed and analyzed using the SHELX software package. The DFT calculations were conducted using the VASP program. The shape and size of the single crystal was shown in the coordinate paper

with a thickness of 0.5 mm ± 0.05 mm. To compare the performance of the single crystal, load-force-dependent indentation depth, time-resolved PL spectra, X-ray response, I-V and I-T curves were tested at least five times, respectively. The XPS spectra were carefully corrected with the binding energy of C 1s. The error bars of the fitted deformation potential (D), decay time, and $\mu\tau$ product value were directly given in the main text by Origin 8.5 program. Since other data were directly obtained, no data processing or statistic procedures were applied.

Supplementary Note I:

Deformation potential (*D*) calculation. The thermal broadening of the PL spectra stems from the fluctuation of the bandgap, which is caused by the displacement of the atoms in the crystal. Therefore, the temperature dependent FWHM is governed by the strength of electron-phonon coupling. The deformation potential (*D*), defined as the change in the bandgap energy per unit strain due to phonon scattering, has been used to describe the electron-phonon interaction.[9] The following model was used to fit the temperature-dependent FWHM[10]:

$$FWHM = \Gamma_0 + \frac{\Gamma_{\text{homo}}}{e^{\frac{\hbar\omega_{\text{homo}}}{k_B T}} - 1}$$

where

$$\Gamma_{\text{homo}} = \frac{\hbar M \omega_{\text{homo}}}{\rho L}\left(\frac{D}{\hbar\omega_{\text{homo}}}\right)^2\left(2 - \mathrm{e}^{-\frac{\hbar\omega_{\text{homo}}}{k_B T}}\right)$$

and Γ_0 is the inhomogeneous linewidth due to structure disorder, M is the sum of the electron and hole effective masses, ω_{homo} is the homopolar phonon frequency and D is the deformation potential. Γ_{homo} can be approximated as

$$\Gamma_{\text{homo}} = \frac{\hbar M \omega_{\text{homo}}}{\rho L}\left(\frac{D}{\hbar\omega_{\text{homo}}}\right)^2$$

Then the model can be expressed in the following form:

$$FWHM = \Gamma_0 + \frac{\frac{\hbar M \omega_{\text{homo}}}{\rho L}\left(\frac{D}{\hbar\omega_{\text{homo}}}\right)^2}{e^{\frac{\hbar\omega_{\text{homo}}}{k_B T}} - 1}$$

the ω_{homo} homopolar phonon mode for the Pb-Br-Pb stretch is ~130 cm^{-1} [11]. Densities (ρ) of for perovskites were calculated using the unit-cell volume measured from single crystal XRD (2.987 g cm^{-3} for $EPZPbBr_4$ and 3.125 g cm^{-3} for $BDAPbBr_4$). The width of the quantum well (L) was quantified using the thickness of the Pb-Br-Pb inorganic layer (1.02 nm for $EPZPbBr_4$ and 0.68 nm for $BDAPbBr_4$).

Supplementary Note II:

The gain factor (G), can be understood as the charge collection efficiency and is calculated by the formula:

$$G = I_R / I_P$$

where I_P is the signal current and I_R is the theoretical current. I_P can be calculated from the formula

$$I_P = \varphi \beta e$$

where φ is the photon absorption rate, defined as,

$$\varphi = \epsilon D m_s / E_{ph}$$

where ϵ is the fraction of absorbed photons, D is the dose rate, m_s is the sample mass, and E_{ph} is the X-ray energy. β is the maximum number of photogenerated carriers, given by:

$$\beta = E_{ph} / \Delta$$

Δ is the ionization energy and calculated by the empirical model as $\Delta=1.43+2E_g$.

Table S1 The occupying volume of the organic ligand for <110>-oriented 2D perovskites within the octahedra-enclosed "half-pocket" cavity.

Materials	a-axis (Å)	b-axis (Å)	c-axis (Å)	Occupying volume (Å^3)
3APrPbBr$_4$	3.4	4.2	4.7	67.116
EDBEPbBr$_4$	3.1	4.6	3.4	48.484
N-MEDAPbBr$_4$	2.45	3.3	4.8	38.808
2AMSPbBr$_4$	4.3	3.3	2.9	41.151
APIPbBr$_4$	3.2	5.25	3.9	65.52
EPZPbBr$_4$	3.8	4.2	5	79.8
EPZPbBr$_4$ add -CH$_3$	3.5	4.4	5.9	90.86
EPZPbBr$_4$ reduce -CH$_3$	3.7	3.7	3	41.07
Octahedra-enclosed "half-pocket" cavity	4.9	4.4	6	129.36

The volume of octahedra-enclosed "half-pocket" cavity is calculated as follows：

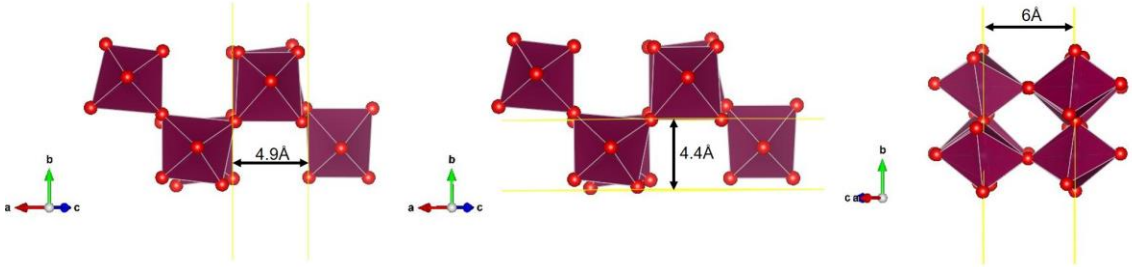

Table S2 Crystal data and structure refinement for $EPZPbBr_4$ single crystal.

Empirical formula	$(C_6H_{16}N_2)PbBr_4$
Formula weight	643.04
Temperature	295K
Wavelength	1.54184 Å
Crystal system	Monoclinic
Space group	P2/c
Unit cell dimensions	a=10.5477 Å, α=90° b=12.4246 Å, β=96.733° c=16.4302 Å, γ=90°
Volume	2138.34(3) $Å^3$
Z	2
Density (calculated)	2.987 g/cm^3
F(000)	1722
Index ranges	＜h＜13 ＜k＜15 ＜l＜20
R indices (all data)	R1=0.0262, wR2=0.0703

Table S3 Crystal data and structure refinement for 2AMSPbBr$_4$ single crystal.

Empirical formula	$(C_3H_{11}SN_3)PbBr_4$
Formula weight	648.01
Temperature	293K
Wavelength	0.71073 Å
Crystal system	Monoclinic
Space group	P21/c
Unit cell dimensions	a=13.2976 Å, α=90° b=8.5472 Å, β=90.439° c=11.9843 Å, γ=90°
Volume	1362.06(16) Å^3
Z	4
Density (calculated)	3.160 g/cm^3
F(000)	1152
Index ranges	＜h＜16 ＜k＜10 ＜l＜14
R indices (all data)	R1=0.0264, wR2=0.0671

Table S4 Crystal data and structure refinement for $EDBEPbBr_4$ single crystal.

Empirical formula	$(C_6H_{18}N_2O_2)PbBr_4$
Formula weight	677.02
Temperature	100K
Wavelength	0.71073 Å
Crystal system	Monoclinic
Space group	P21/c
Unit cell dimensions	a=6.0917 Å, α=90° b=28.7804 Å, β=91.852° c=8.886 Å, γ=90°
Volume	1557.09(13) $Å^3$
Z	4
Density (calculated)	2.888 g/cm^3
F(000)	1224
Index ranges	＜h＜7 ＜k＜35 ＜l＜10
R indices (all data)	R1=0.0234, wR2=0.0638

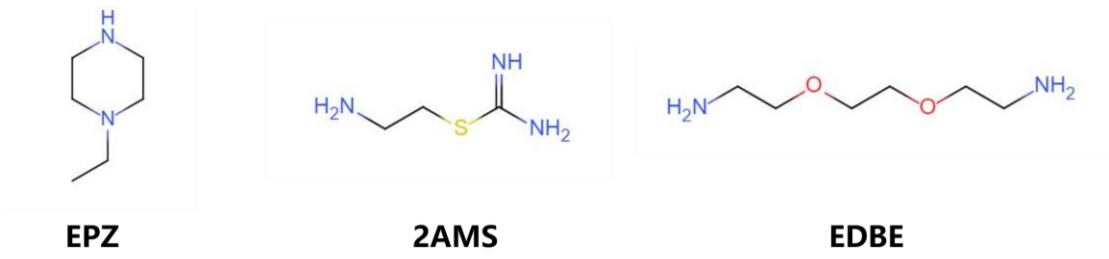

Figure S1 Structure of the organic ligand EPZ (1-ethylpiperazine), 2AMS (2-(aminoethyl)isothiourea) and EDBE (2,2'-(ethylenedioxy)bis(ethylammonium)).

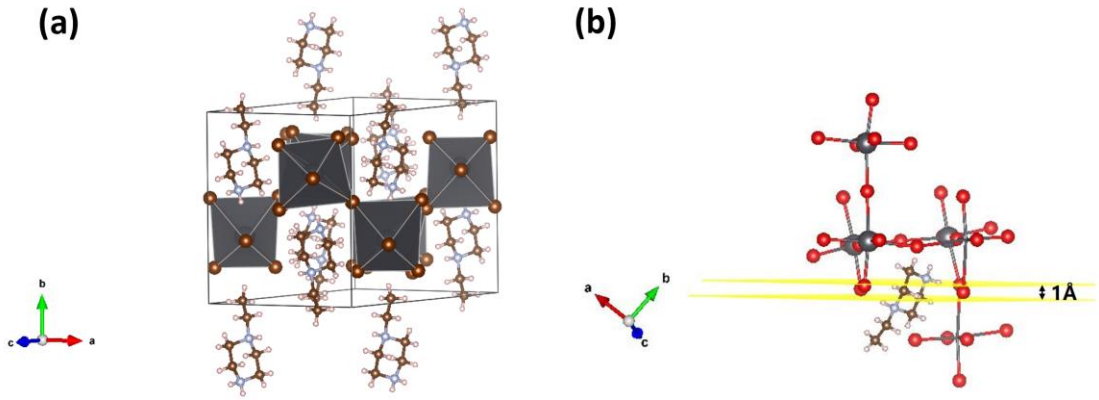

Figure S2 (a) single crystal structure of $EPZPbBr_4$ measured from diffractometer with defined unit cell and corresponding *a*, *b*, *c* directions, (b) The $-NH_3$ penetration depth of $EPZPbBr_4$.

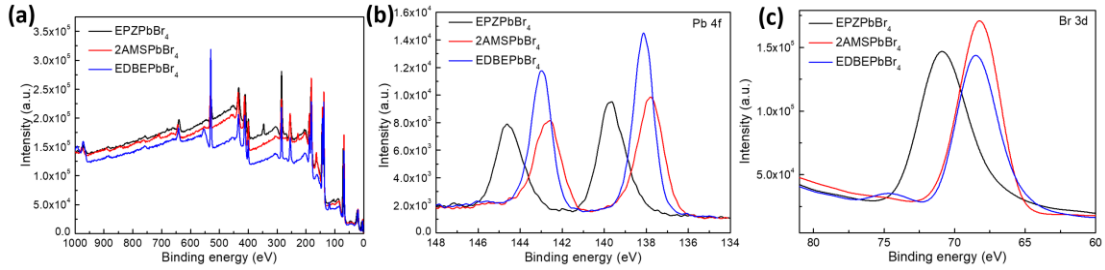

Figure S3 XPS spectra of (a) all elements, (b) Pb 4f, and (c) Br 3d of $EPZPbBr_4$, $2AMSPbBr_4$, $EDBEPbBr_4$

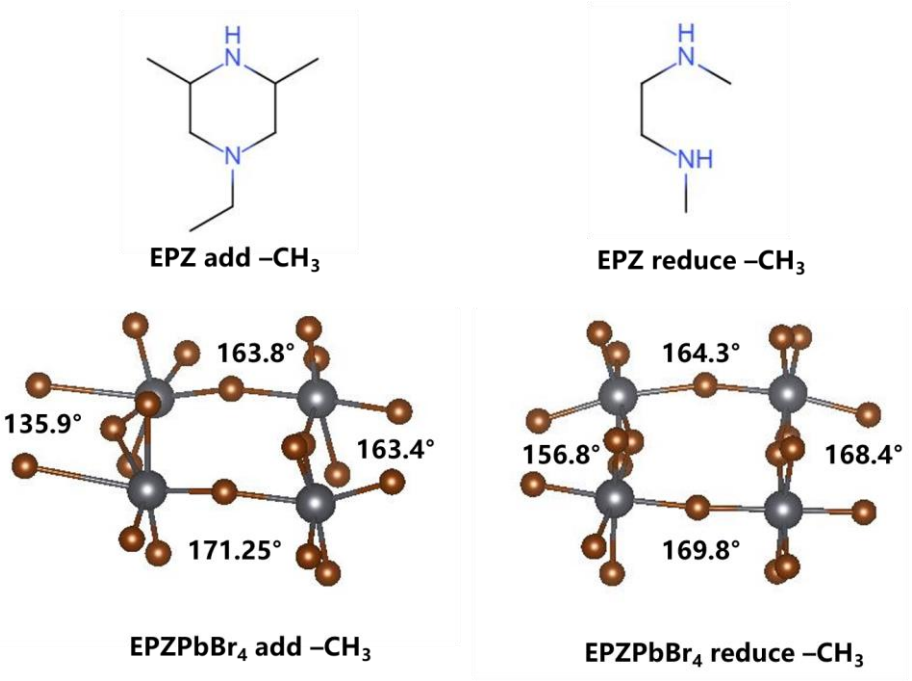

Figure S4 Pb-Br-Pb bond angles of "Add -CH_3" and Reduce -CH_3" $EPZPbBr_4$.

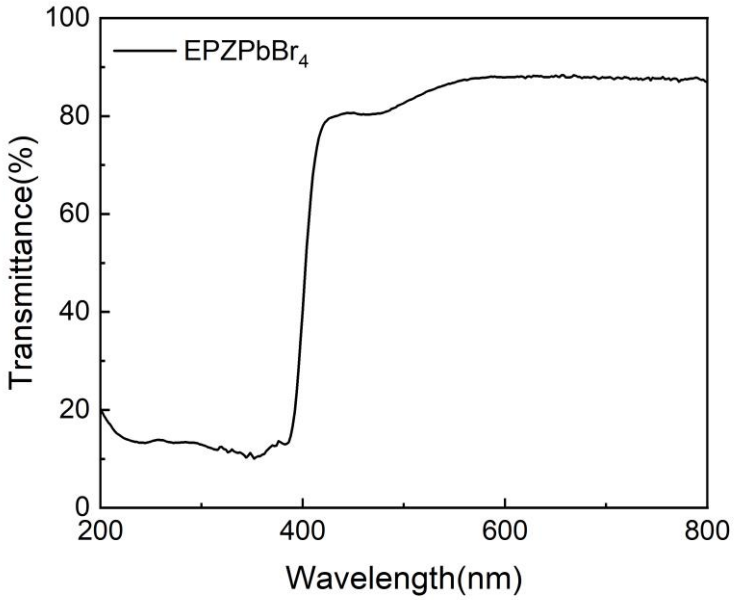

Figure S5 Transmittance spectrum of $EPZPbBr_4$ single crystal.

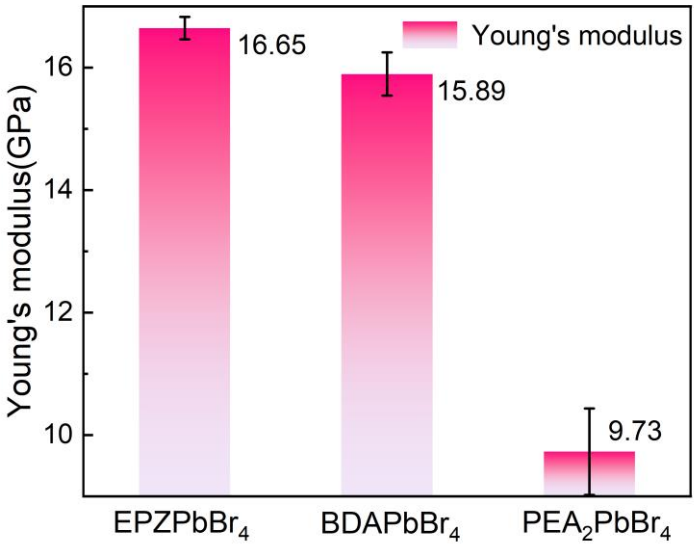

Figure S6 Young's modulus of $EPZPbBr_4$, $BDAPbBr_4$ and PEA_2PbBr_4 single crystals.

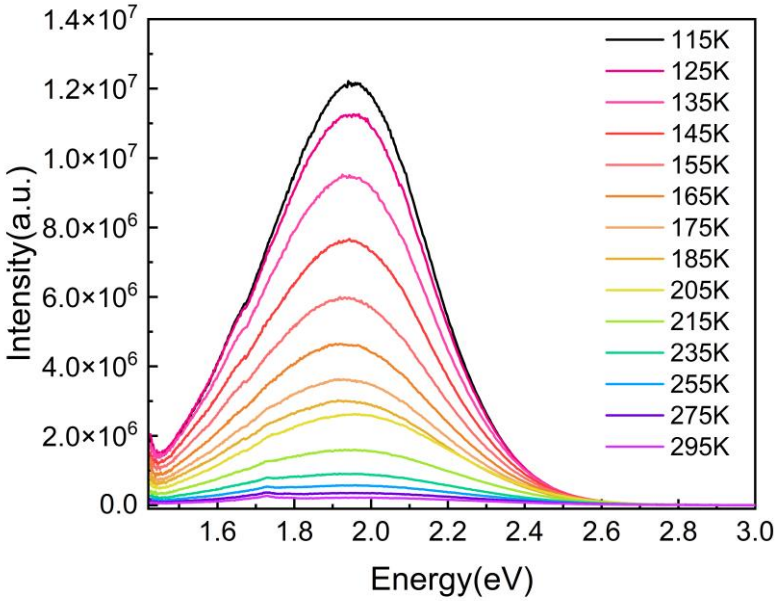

Figure S7 Temperature-dependent photoluminescence spectra of $EPZPbBr_4$ single crystal measured at the temperatures from 115 K to 295 K.

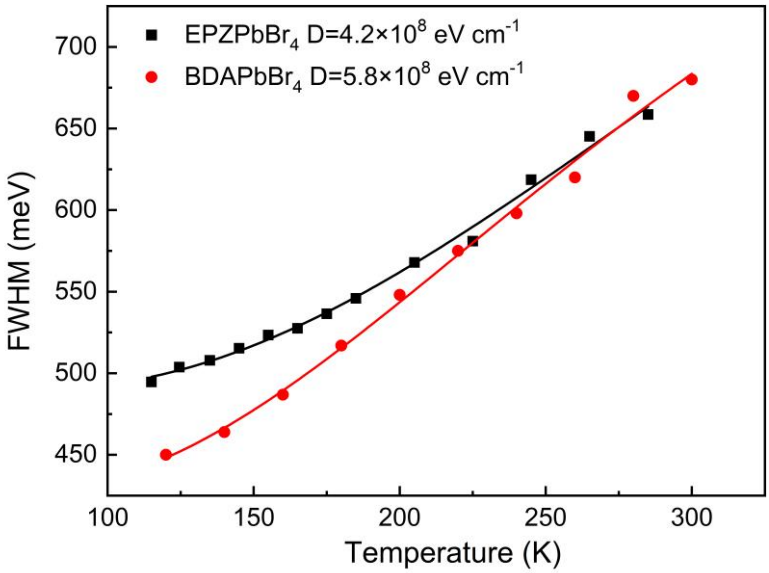

Figure S8 FWHM of the steady-state PL spectra as a function of temperature for EPZPbBr4 and BDAPbBr4 single crystals.

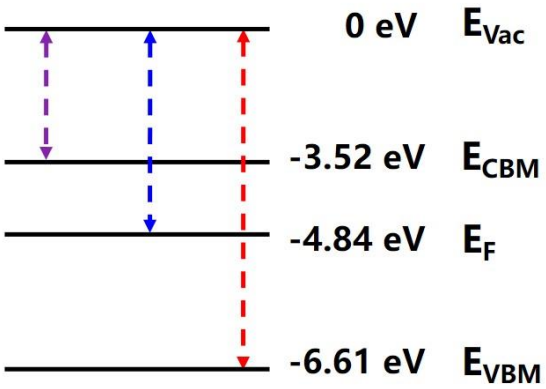

Figure S9 Energy level of of EPZPbBr4.

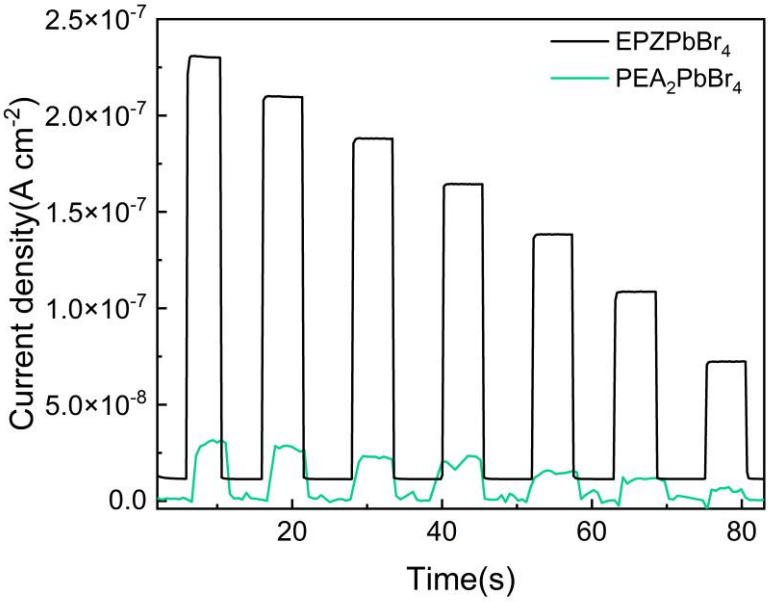

Figure S10 I-T curves of $EPZPbBr_4$, PEA_2PbBr_4 under different X-ray dose rates from 580 to 82.86 μGy s^{-1}.

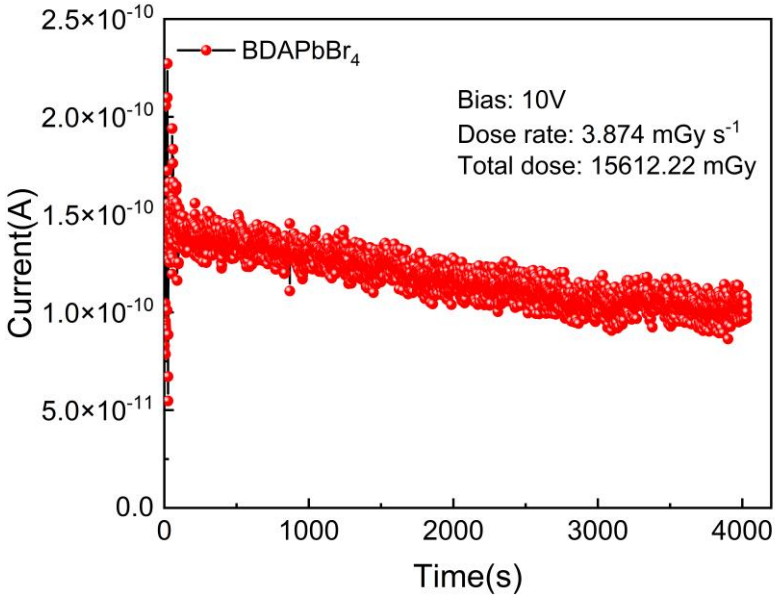

Figure S11 Irradiation stability of $BDAPbBr_4$ exposed to X-rays (3.874 mGy s^{-1}) under 10 V bias voltage.

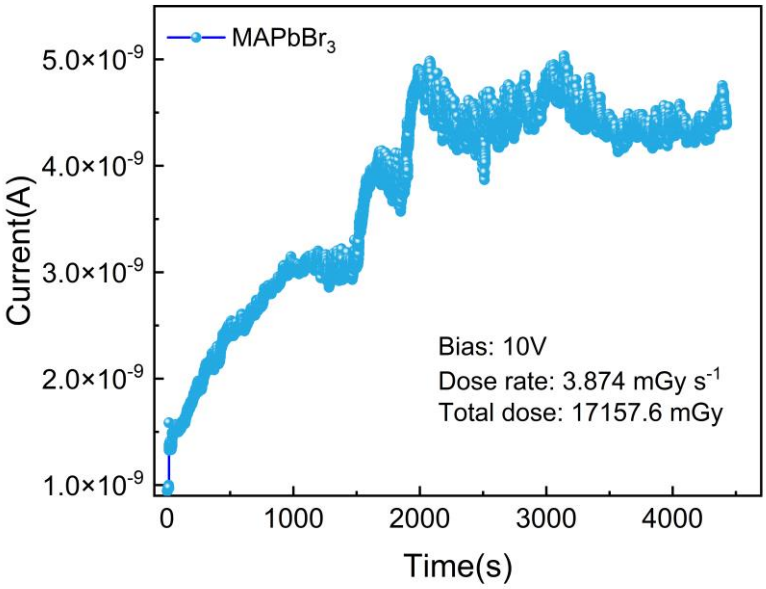

Figure S12 Irradiation stability of $MAPbBr_3$ exposed to X-rays (3.874 mGy s^{-1}) under 10 V bias voltage.

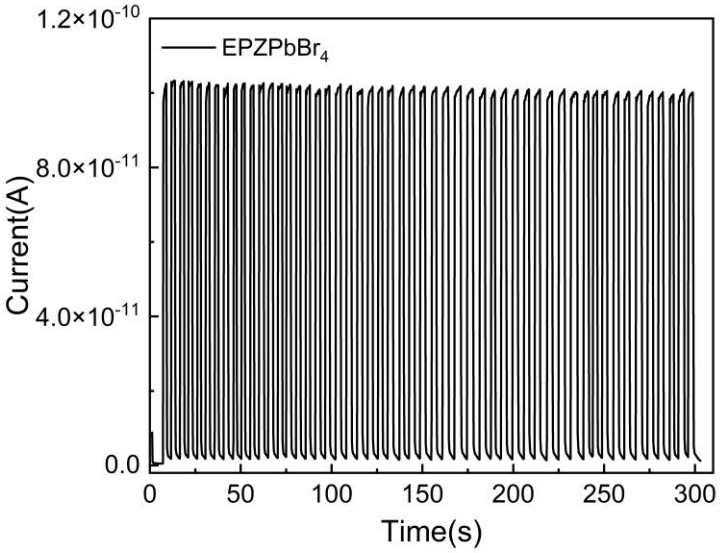

Figure S13 Detectors to on–off X-ray in a test period of about 300 s at 10 V bias (dose rate = 3.874 mGy s^{-1}.

References:

[1] G. Kresse, J. Furthmüller, *Physical Review B* **1996**, 54, 11169-11186.

[2] G. Kresse, J. Furthmüller, *Computational Materials Science* **1996**, 6, 15-50.

[3] P. E. Blöchl, *Physical Review B* **1994**, 50, 17953-17979.

[4] G. Kresse, D. Joubert, *Physical Review B* **1999**, 59, 1758-1775.

[5] H. J. Monkhorst, J. D. Pack, *Physical Review B* **1976**, 13, 5188-5192.

[6] L. G. Ferreira, M. Marques, L. K. Teles, *Physical Review B* **2008**, 78, 125116.

[7] K.-H. Xue, J.-H. Yuan, L. R. C. Fonseca, X.-S. Miao, *Comput. Mater. Sci.* **2018**, 153, 493-505.

[8] G.-Q. Mao, Z.-Y. Yan, K.-H. Xue, Z. Ai, S. Yang, H. Cui, J.-H. Yuan, T.-L. Ren, X. Miao, *J. Phys.: Condens.Matter* **2022**, 34, 403001.

[9] A. Franceschetti, S.-H. Wei, A. Zunger, *Phys. Rev. B* **1994**, 50, 17797-17801.

[10] Z. Guo, X. Wu, T. Zhu, X. Zhu, L. Huang, *ACS Nano* **2016**, 10, 9992-9998.

[11] X. Gong, O. Voznyy, A. Jain, W. Liu, R. Sabatini, Z. Piontkowski, G. Walters, G. Bappi, S. Nokhrin, O. Bushuyev, M. Yuan, R. Comin, D. McCamant, S. O. Kelley, E. H. Sargent, *Nat. Mater.* **2018**, 17, 550-556.